Computational Study on the Mechanism of the Acceleration of 1,3-Dipolar Cycloaddition inside Cucurbit[6]uril

Charles Goehry,[†] Maria Besora,[†] and Feliu Maseras*,[†,‡]

[†]Institute of Chemical Research of Catalonia (ICIQ), Avgda. Països Catalans, 16, 43007 Tarragona, Catalonia, Spain
[‡]Departament de Química, Universitat Autònoma de Barcelona, 08193 Bellaterra, Catalonia, Spain

S *Supporting Information*

ABSTRACT: The enhanced reactivity of the Huisgen 1,3-dipolar cyclo-addition between the protonated forms of azidoethylamine and propargyl-amine inside the cucurbit[6]uril host has been computationally studied. A DFT approach is applied to explore the relative stabilities and connections of a large variety of possible host–guest aggregates that may be formed in solution, as well as their reactivity. The free energies resulting from the DFT calculations are converted to rate and dissociation constants and introduced, together with the experimentally reported initial concentrations, in a kinetic simulation. The results reproduce the experimental observations and provide a detailed description of the behavior of a large host–guest system over time. The major cause of the rate acceleration inside the nanovessel is the reduction of the entropic component of the free energy barrier, and the existence of stable nonproductive host–guest adducts is identified as a major obstacle to improved catalysis.

KEYWORDS: host–guest catalysis, density functional theory, kinetic simulations, cycloaddition, cucurbituril
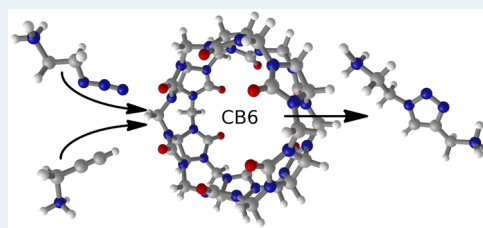
INTRODUCTION

Supramolecular catalysis is a well-established research field that encompasses a variety of catalytic processes where noncovalent binding interactions play an important role.[1–3] A particularly interesting area of supramolecular catalysis is that of host–guest catalysis, where the reactants are introduced in a supra-molecular nanovessel, or molecular container,[4] where the reaction takes place with a rate higher than that outside the supramolecule. Host–guest catalysis has an appealing intuitive connection to enzymatic catalysis, which is well-known for its high efficiency,[3,5] and has been applied successfully in a variety of systems.[6–11] A further expansion of host–guest catalysis would in any case be largely helped by a better mechanistic understanding of the processes.

Computational chemistry has been a very successful complement to experiment in the mechanistic clarification of transition-metal homogeneous catalysis,[12–15] but its application in host–guest catalysis has been rather modest so far, the major focus being on the encapsulation process[16–18] but not on the acceleration mechanism.[19,20] One of the reasons for this limited application may be the mechanistic complexity of this type of process. Direct comparison of transition state free energies is a useful procedure for the treatment of sequential processes like those often involved in enantioselectivity,[21] but it is too simplistic for complicated networks involving ramifications and loops. The use of kinetic models becomes mandatory in this case. Although their use is well established in heterogeneous catalysis,[22] their application in homogeneous systems has been more scarce.[23]

In this work, we will explore computationally the mechanism of the 1,3-dipolar cycloaddition between the protonated forms of azidoethylamine $NH_3^+CH_2CH_2N_3$ (**A**) and propargylamine $NH_3^+CH_2C\equiv CH$ (**B**) inside a cucurbit[6]uril nanoreactor, CB6 (**E**). This process was experimentally explored by Mock and co-workers[24,25] and constitutes still today one of the most successful examples of reaction acceleration inside a molecular host. CB6 is a rigid macrocycle constituted of six glycoluril monomers linked by methylene bridges.[26] It has a torus shape about 10 Å wide and 6 Å high, forming a partially enclosed cavity. Small solvent or solute molecules can access its hydrophobic center through the two openings. Each rim is surrounded by six carbonyl dipoles, which constitute the cation binding site.[27–29] The uncatalyzed 1,3-dipolar Huisgen cyclo-addition produces 1,4- and 1,5-substituted triazoles, in different mixtures depending on the reactants and experimental conditions.[30,31] The reaction inside the nanoreactor CB6 does produce selectively the 1,4-substituted triazole. Similar to what is observed for the copper-catalyzed "click" reaction,[32] the cycloaddition inside the CB6 was found to be accelerated 5.5×10^4 fold. A wealth of mechanisms and kinetics for the system were provided in the original experimental reports.[24,25]

We carried out an initial computational study on the reactivity of this system,[19] but we focused only on the reaction once the guests are inside the host. Other computational studies on cucurbit[n]urils have focused on the binding of a variety of guests: halogens,[33] octane and adamantane derivatives,[34,35] cyanine dyes,[36] antitumor platinum drugs,[37] and actinyl cations.[17] None of these previous computational

studies analyzed the process leading to the formation of a reacting complex inside the capsule and its influence on the overall acceleration rate. We address the topic in this work with the application of DFT calculations and of a kinetic model.

■ COMPUTATIONAL DETAILS

Electronic structure calculations were carried out with the Gaussian 09 suite of programs.[38] Geometry optimizations in the gas phase were carried out using the B97D functional[39] together with the 6-31G(d) basis set BS1.[40] Frequency calculations at this same level were carried out to confirm the nature of the stationary points located as minima or transition states. The functional and basis set for the final energy evaluation were chosen through separate calibration processes detailed in the Supporting Information. For the functional, B3LYP, PBE, M06, B97D, and B97D3 were evaluated, the final choice being B97D3.[41] This fits well with the good performance reported for this method in pericyclic reactions.[42] For the basis set, 6-31G(d), 6-311G(d), 6-311+G(d), 6-311+G(d,p) and 6-311++G(d,p) were evaluated. We finally settled on 6-311G(d) (BS2)[43] providing the best quality/price ratio. A comparison between results with different basis sets suggests that the error in computed energies should not be larger than 2.0 kcal/mol.

Experimentally a mixture of water and formic acid was used as solvent. Solvent effects were taken into account by two means: (i) up to two formic acid molecules were included explicitly in the reaction network, and (ii) solvent corrections were applied to all species through single-point calculations using the continuum model SMD for water, as implemented in Gaussian 09.[44] Test calculations were performed to confirm the validity of our approach to model the solvent effects. We tested water and formic acid as guests for CB6, and we found that only one or two molecules of formic acid interact favorably with the macrocycle. More molecules or any number of water molecules display positive free energies of complexation. We are aware that water molecules cannot be a priori discounted as guests in supramolecular complexes, as the hydrophobic effect has been put into question,[45] but our explicit tests show no binding of water in our specific system.

All reported interaction energies between fragments have been corrected for basis set superposition error (BSSE) using the counterpoise scheme.[46] Free energy contributions were obtained from frequency calculations with the small basis set, and a correction term for changing the standard state from 1 atm to 1 M (1.89 kcal/mol per molecule) was applied to all free energy calculations. Unless mentioned otherwise, all reported energies are thus gas phase free energies corrected with solvation effects, standard state corrections, and BSSE. Geometry optimizations and frequency calculations are done with the small basis set BS1, while final energies and all other corrections are obtained with the larger BS2.

The kinetic analysis was carried out with the programs Acuchem[47] and Tenua,[48] which produce identical results, negligible accumulation of numerical errors aside. Rate constants were estimated through the Eyring equation[49] from the free energy of activation (see the Supporting Information for further details). The initial concentrations of reactants were introduced according to experimental data.

■ RESULTS

Reaction Overview. We studied computationally the reaction between the protonated forms of azidoethylamine (**A**) and propargylamine (**B**) mediated by cucurbit[6]uril (CB6, **E**). The reaction is expected to proceed following the scheme in Figure 1. First, the two reactant guests, **A** and **B**, are trapped
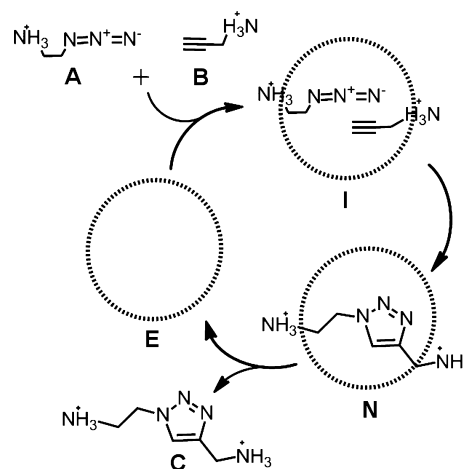
Figure 1. Catalytic cycle for the reaction between azidoethylamine (**A**) and propargylamine (**B**) mediated by the host cucurbit[6]uril (CB6, **E**). The CB6 macrocycle is represented by a bold dashed circle.

inside the CB6 host, forming aggregate **I**. Once species **I** is formed, the cycloaddition between the azide and acetylene takes place, forming the triazole product inside the CB6 macrocycle, species **N**. Species **N** could liberate the triazole **C** and recover the CB6 host **E**, but this is not experimentally observed, as the guest product remains inside the host.[24]

Our procedure for the modeling of the process consisted of four main steps: (i) geometry optimization and calculation of the relative Gibbs free energies of all of the compounds of interest and the transition states (TS) linking them, (ii) building of a reaction network containing all of the relevant elementary reactions, (iii) conversion of activation free energies into rate constants, and (iv) use of a kinetic program to integrate all data. This provided a kinetic model that should be able to explain the behavior of the global system over time.

DFT Calculations. The core of the process is the reaction between guests **A** and **B**, which was thus first analyzed. The potential energies (V) and free energies (G) of the species involved in the reaction outside and inside the capsule are collected in Table 1. For the reaction inside the host **E**, there are three types of productive aggregates: **F** with **A** trapped alone by the host, **J** with **B** trapped alone, and **I** with both substrates trapped by the macrocycle (see Figure 2). Other stable but nonproductive aggregates (**G**, **H**, **K**, **L**, or **M**) can also be formed and will be discussed later.

Alkyne binding to the capsule (**J**, −14.2 kcal/mol) is preferred over azide binding (**F**, −7.9 kcal/mol). Trapping the two guests simultaneously (**I**, −7.9 kcal/mol) is not favored over trapping one of them in terms of free energy. It can be observed in Figure 2 that the guests push each other when held together inside the capsule. As can be seen in Table 1, in terms of potential energy (roughly equivalent to enthalpy), **I** is more stable than either **F** or **J**, but the entropic cost of bringing three fragments together overcomes this stabilization.

Table 1. Potential Energies (V) and Free Energies (G) for Species Involved in the Cycloaddition outside and inside the Capsule[a]

	relative energy	
	V_{sol}	G_{sol}
A + B + E	0.0	0.0
F + B	−24.5	-7.9
J + A	−28.7	-14.2
I	−39.7	-7.9
TS(AB-C)	14.6	26.1
TS(I-N)	−29.3	6.1
	reaction barrier	
	$\Delta V^{\ddagger}_{sol}$	$\Delta G^{\ddagger}_{sol}$
A + B → C	14.6	26.1
I → N	10.4	14.0
J + A → N	−0.6	20.3

[a]Values in kcal/mol.
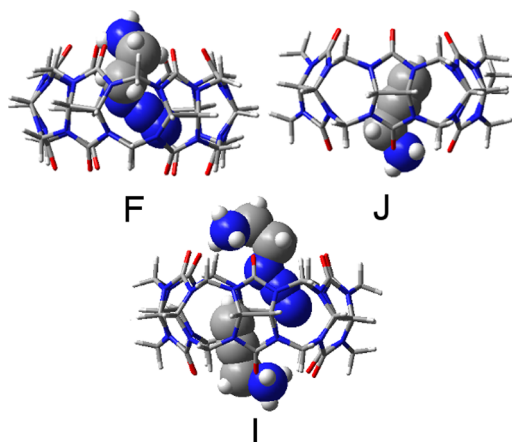
Figure 2. Structures of the productive aggregates **F**, **J**, and **I**.

The 1,3-dipolar cycloaddition transition states are concerted, forming the two new C−N bonds simultaneously, both inside (**TS(I-N)**) and outside (**TS(AB-C)**) of the capsule. The energies of these TSs are presented also in Table 1, together with the computed barriers for the processes. The barrier for the reaction outside the capsule is 14.6 kcal/mol in potential energy and 26.1 kcal/mol in free energy. The free energy value is slightly lower than the 31.0 kcal/mol reported in a previous study from our group,[19] and the differences can be attributed to the method (lack of dispersion and BSSE in the older study). Two different barriers are presented for the reaction inside the capsule, one measured from the encapsulated adduct **I** and the other from the lowest free energy point **J + A**. The reason for introducing the first value is to allow the most intuitive comparison with the reaction outside the capsule. The barrier from **I** to **TS(I-N)** is 10.4 kcal/mol in potential energy and 14.0 kcal/mol in free energy. Again, the free energy barrier is lower than the 17.9 kcal/mol previously reported, but the trend is the same. Remarkably, the difference between both reactions we highlighted in our previous publication holds here, as the change in the entropic contribution is critical. The difference between potential energy and free energy barrier for the uncatalyzed reaction is 11.5 kcal/mol (26.1 minus 14.6), while the corresponding difference inside the capsule is 3.6 kcal/mol (14.0 minus 10.4). The difference between potential energy and free energy corresponds mostly to the entropic term and is

substantially reduced when the process takes place inside the capsule.

Although useful for discussion, the barrier between **I** and **N** is not critical to the process, because **I** is not the most stable adduct previous to the transition state. The most stable set of species is **J + A**, with the alkyne inside the capsule and the azide outside. The free energy barrier from this species to the transition state is 20.3 kcal/mol, still lower than that for the reaction without the capsule. The presence of additional species that must have an effect on the overall kinetics hints to a more complicated process than expected, and because of this we explored other possible species in the reaction media.

Species **N** with the product inside the capsule is thermodynamically very stable, located at −65.1 kcal/mol relative to separate reactants. Liberation of the product **C** and recovery of **E** from **N** has a cost of 18.8 kcal/mol. This means that **C** binds more strongly to the CB6 host than **A**, **B**, or the combination of them and is consistent with the fact that **N** is the resting state in the experimental process.

The productive species mentioned above are not the only ones present in the reaction media. A large amount of nonproductive species are relevant in the reaction network of this system.[24] There can be up to two guests trapped in the macromolecule and up to two formic acid molecules (solvent), as CB6 has two openings. We also considered the possible inclusion of water molecules,[45] but their binding was not favored in our system.

One example of nonproductive aggregate is presented in Figure 3. **M** is an aggregate which presents two molecules of
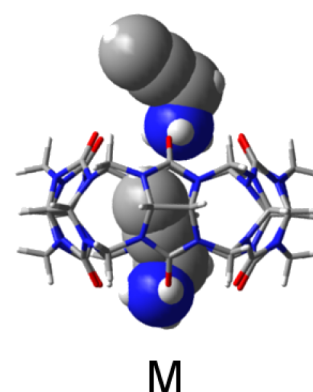
Figure 3. Illustration of nonproductive binding. There are two alkynes inside the cavity.

alkyne **B** binding to CB6; it is located at −17.1 kcal/mol. This species is more stable than the productive aggregate **J** reported above. There are many more possible species. They are presented in Figure 4, together with a simplified version of their connectivity network, following a symbolic code. Different species are represented as objects with different shapes and colors: a black dashed circle for CB6, elongated balloons for azide **A** (dark blue) and alkyne **B** (light blue), and ellipsoids for formic acid (small and gray) and the 1,4-product (dark green). Two host−guest bonding modes are distinguished by the orientation of the balloon: inward for productive binding and outward for nonproductive binding. As mentioned above, water does not appear in this scheme as a guest because we found that for our system complexes involving water were less stable than complexes involving no solvent or formic acid.
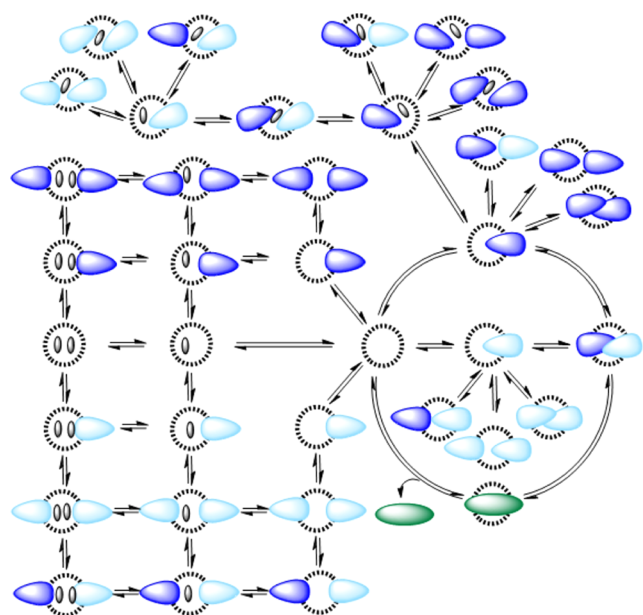
Figure 4. Simplified network of computed minima related to CB6 and its guests (**A** and **B** and formic acid as solvent). Structures are in dynamic equilibrium. For simplicity, not all possible connections between species are included.

Kinetic Model. After initial inspection of the species in the network depicted in Figure 4, we discarded those with free energies that were too high and applied the kinetic model to the scheme depicted in Figure 5. The rate constants for the cycloaddition steps reported above were obtained from application of the Eyring equation. For the barrierless processes of aggregation and disaggregation, we assumed diffusion control and used a rate constant $k_{\text{diff}} = 1.1 \times 10^{11}$ M^{-1} s^{-1}, which corresponds to a pseudo activation free energy of $\Delta G^{\ddagger} = 2.4$ kcal/mol (further details on this approach are provided in the Supporting Information).

The results of the kinetic simulation are summarized in Figure 6. The graph represents the evolution of the
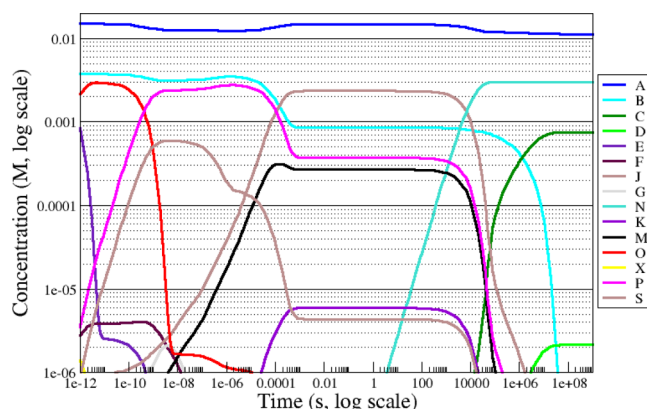
Figure 6. Evolution of the concentration of the most relevant species related to CB6 and its guests over time. Only species with a concentration between 10^{-6} and 0.1 M are included in the plot.

concentration of the different chemical entities over time, using a logarithmic scale on both axes. Only the most relevant species appear for clarity. The initial concentrations, taken from the reported experimental data,[24] are 0.0150, 0.00375, and 0.0030 M for **A**, **B**, and **E**, respectively. As some aggregates involve solvent (formic acid) molecules, this is included with a concentration of 11.6 M. The concentration of **A** is high through the whole time scale because this reactant is in excess, with concentration 4 times larger than that in **B**. The empty macrocycle, **E**, quickly disappears in favor of other aggregates. In the very early stages of the process, these aggregates coexist with a significant amount of **B**. This is the case for aggregate **O** (from 10^{-12} to 10^{-9} s) and **P** (from 10^{-9} to 10^{-3} s). After 10^{-3} s, **J** becomes the dominant species, clearly displacing **B**, and it remains as main species coexisting with the other reactant **A** until 10^{4} s (i.e., about 4 h), at which time the cycloaddition takes place inside the capsule and **N** is formed. **N** remains as the final product on all the time scales considered, although the concentration of free cycloaddition product **C** trends up until reactant **B** is fully consumed. We notice also the appearance of the minor product, the 1,5-regioisomer, in the last stages of the
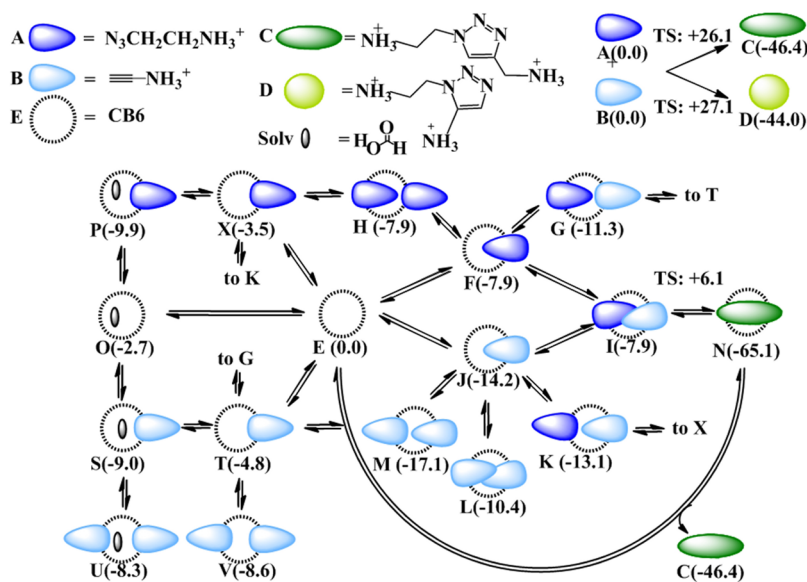
Figure 5. Pruned network of structures selected for the kinetic model. Most stable structures and relevant intermediates have been selected. Free energies are given in kcal/mol.

Table 2. Comparison of Experimental Original Data, Reinterpreted Data from Experiments, and Computational Data[a]

reaction	original data[b]			reinterpreted data[b]			computational data[c]	
	k or K_d	ΔG	$\Delta G^{\ddagger}$	k or K_d	ΔG	$\Delta G^{\ddagger}$	ΔG	$\Delta G^{\ddagger}$
A + B → C + D	1.2×10^{-6}		27.3^d	1.2×10^{-6}		27.3^d		26.1/27.1
A + B → C								26.1
A + B → D								27.1
F ⇌ E + A	2.5×10^{-3}	3.7					7.9	
J ⇌ E + B	6.5×10^{-4}	4.6					14.2	
cpF ⇌ F + cp				2.5×10^{-3}	3.7		3.1	
cpJ ⇌ J + cp				6.5×10^{-4}	4.6		3.5	
M ⇌ J + B	3.0×10^{-1}	−0.7					2.9	
I ⇌ J + A	3.0×10^{-1}	−0.7					−6.3	
1/2(M + I ⇌ 2J + A + B)				3.0×10^{-1}	-0.7^f		-1.7^e	
I → N	1.9×10^{-2}		20.8					14.0
J → N				1.9×10^{-2f}		20.8^f		20.3

[a]K_d is the dissociation constant. [b]Free energies obtained at the experimental temperature $T = 313.15$ K. [c]Free energies computed at $T = 298.15$ K. [d]Averaged value, assuming that both reactions (**A + B → C** and **A + B → D**) have the same rate constant. [e]Averaged value, to reproduce the experimental assumption of two identical rate constants for **A** and **B**. [f]Values reinterpreted from raw experimental kinetic data.

reaction, although with concentrations always well below 10^{-5} M. We confirmed through additional kinetic simulations that this minor product is generated outside the capsule, through the uncatalyzed reaction.

The logarithmic scale in both axes of Figure 6 is useful to have a global view of the system evolution, but one has to realize that the times and concentrations used on a practical human scale represent a small area of the overall plot. Notice, for example, that 10^9 s is roughly equivalent to 32 years. Thus, from a practical point of view, reactant **B** is transformed in a near-quantitative way into aggregate **J** in less than 1 s, and it remains in that form until it evolves toward the encapsulated product **N** in a few hours. Although no detailed data on reaction time are provided in the experimental report,[24] the time scale resulting from our calculation seems reasonable for a reaction occurring in the laboratory.

Species **J**, represented in Figure 2, contains one alkyne molecule inside the capsule. Its key role in the catalytic cycle is remarkable, as species **M** (Figure 3) with two alkynes inside the cavity has a free energy lower by 2.9 kcal/mol. The preference of **J** over **M** is related to concentration effects; the concentration of free alkyne **B** becomes low during the process and shifts the equilibrium from **M** to **J**. The kinetic model is thus shown to be useful for the identification of the key species in the reactivity of the system.

Kinetic simulations can be also used to see how the behavior of the system may be affected by modifications in the initial concentrations or other conditions. We made one of these tests by changing the concentration of formic acid, which may be possible to easily adjust experimentally. The results, collected in the Supporting Information, indicate very minor changes in the key features of the overall process for this particular modification.

Comparison between Experimental and Theoretical Data. The experimental report[24] contained a great deal of thermodynamic and kinetic data that should in principle be reproduced by our microscopic description of the system. We carry out this comparison in Table 2. The dissociation constants and kinetic constants have been converted into energy differences (ΔG) and activation energies ($\Delta G^{\ddagger}$),

respectively; details of the conversion are provided in the Supporting Information. The results in Table 2 are organized in three vertical blocks and four horizontal blocks. The vertical block at the left contains values reported in the experimental paper, with the vertical block at the right containing the values for these same reactions from our calculations. There is reasonable agreement in the first horizontal block, the uncatalyzed reaction (experiment 27.3 kcal/mol vs computation 26.1/27.1 kcal/mol). However, the agreement is poor in all other horizontal blocks. This is in contrast with the satisfactory results reported above from the kinetic simulation, and because of this we decided to analyze in more detail the different parameters. Our conclusion is that the rate constants and dissociation constants reported in the experimental work are the result of a number of assumptions, which were perfectly reasonable but which can be revised in view of the detailed mechanism. The central vertical block of Table 2 contains our reinterpretation of the experimental raw data.

The second horizontal block concerns the decomplexation of **F** (**F ⇌ E + A**) and **J** (**J ⇌ E + B**). This consists of the departure of each of the reactants from the species where one of them is contained inside the capsule. The dissociation rates reported in the experimental work were obtained from independent complexation experiments that measure the displacement of a known calibrating guest (the bulky chromophore guest **cp**) by the guest under study. Kinetic data were interpreted by assuming a dissociative mechanism for this process.[50] We carried out additional calculations on the displacement reaction (reported in the Supporting Information) and found out that the mechanism is not dissociative. The new species **cpF** and **cpJ** are formed, and we postulate that the experimentally reported dissociation constant corresponded in fact to departure of the guest from these complexes. When these are taken into account, the computed results are within 1.1 kcal/mol of experiment.

The third horizontal block concerns the dissociation constants of **M ⇌ J + B** and **I ⇌ J + A**. These are processes where the host containing two guests loses one of them, and both processes had been assumed to have similar dissociation constants. According to our calculations, they differ by 9.2 kcal/

mol. However, the reported experimental value is close to the average of the two computed values.

The fourth horizontal block concerns the cycloaddition step from the previous stable adduct ($\mathbf{I} \rightleftharpoons \mathbf{N}$). This adduct was considered to be **I**, with two guest molecules, in the experimental paper, but we have found here that **J**, with only one guest, is more stable. Correcting the origin of energies for this barrier again brings the experimental value close to calculation.

Therefore, a reintepretation of the experimental data brings them to close agreement with calculation. This reinterpretation is by no means a criticism of the work in the experimental report. All assumptions made were reasonable, and their chemical conclusions are proved correct by our calculations. The reinterpretation is simply necessary in view of the detailed mechanistic picture that could not be accessed from pure experimental data.

CONCLUSIONS

Computational chemistry is able to build a detailed mechanistic picture of a complex process of host-catalyzed cycloaddition that reproduces all available experimental data. DFT calculations on the key cycloaddition step must be complemented by a systematic search of possible nonproductive adducts, and all of the DFT results must be included on a kinetic model.

The results confirm that a major part of the catalytic effect of encapsulation on a reaction between two fragments is the reduction of the entropic cost of bringing them together.[19,24] This poses a limit on the maximum acceleration that can be achieved, as the entropic term is often between 10 and 15 kcal/mol at most, but this type of increase in rate would be largely sufficient for most practical applications. The real hindrance to rate acceleration of the cycloaddition that has been studied lies in the existence of stable nonproductive adducts. Our kinetic model showed that the system evolved immediately to a nonproductive adduct with only one reactant inside the capsule and that the cycloaddition step could only take place upon slow evolution from this adduct to the productive adduct with the two reactants in a productive orientation.

Apart from the reproduction of the experimental results, the calculation also provides a detailed microscopic view of the mechanism that can be useful in the reevaluation of some assumptions in the estimation of experimental rate and dissociation constants. In this way, calculation complements experiment and may open the way to the design of more efficient processes. With this idea in mind, we are currently working on the extension of this computational treatment to other problems in host−guest catalysis.

ASSOCIATED CONTENT

Ⓢ Supporting Information

The following file is available free of charge on the ACS Publications website at DOI: 10.1021/cs501703t.

> Conversion formulas between free energies, rate constants, and dissociation constants, information on the handling of diffusion-controlled processes, calibration of functionals and basis sets for this system, calculations with the chromophore guest, evolution of concentrations in a computational experiment with reduced formic acid, and Cartesian coordinates and potential energies for all computed species (PDF)

AUTHOR INFORMATION

Corresponding Author

*E-mail for F.M.: fmaseras@iciq.es.

Notes

The authors declare no competing financial interest.

REFERENCES

(1) Nitschke, J. R. *Chem. Soc. Rev.* **2014**, *43*, 1798−1799.
(2) Raynal, M.; Ballester, P.; Vidal-Ferran, A.; van Leeuwen, P. W. N. M. *Chem. Soc. Rev.* **2014**, *43*, 1660−1733.
(3) Raynal, M.; Ballester, P.; Vidal-Ferran, A.; van Leeuwen, P. W. N. M. *Chem. Soc. Rev.* **2014**, *43*, 1734−1787.
(4) Ballester, P.; Fujita, M.; Rebek, J. *Chem. Soc. Rev.* **2015**, *44*, 392−393.
(5) Dong, Z.; Luo, Q.; Liu, J. *Chem. Soc. Rev.* **2012**, *41*, 7890−7908.
(6) Kirby, A. J. *Angew. Chem., Int. Ed. Engl.* **1996**, *35*, 706−724.
(7) Conn, M. M.; Rebek, J. *Chem. Rev.* **1997**, *97*, 1647−1668.
(8) Hof, F.; Craig, S. L.; Nuckolls, C.; Rebek, J. *Angew. Chem., Int. Ed.* **2002**, *41*, 1488−1508.
(9) Meldal, M. *Angew. Chem., Int. Ed.* **2005**, *44*, 7829−7830.
(10) Pluth, M. D.; Bergman, R. G.; Raymond, K. N. *Acc. Chem. Res.* **2009**, *42*, 1650−1659.
(11) Hastings, C. J.; Pluth, M. D.; Bergman, R. G.; Raymond, K. N. *J. Am. Chem. Soc.* **2010**, *132*, 6938−6940.
(12) McMullin, C. L.; Jover, J.; Harvey, J. N.; Fey, N. *Dalton Trans.* **2010**, *39*, 10833−10836.
(13) Balcells, D.; Clot, E.; Eisenstein, O. *Chem. Rev.* **2010**, *110*, 749−823.
(14) Sameera, W. M. C.; Maseras, F. *WIREs Comp. Mol. Sci.* **2012**, *2*, 375−385.
(15) Thiel, W. *Angew. Chem., Int. Ed.* **2014**, *53*, 8605−8613.
(16) Tovilla, J. A.; Carlqvist, P.; Benet-Buchholz, J.; Maseras, F.; Vilar, R. *Supramol. Chem.* **2007**, *19*, 599−611.
(17) Sundararajan, M.; Sinha, V.; Bandyopadhyay, T.; Ghosh, S. K. *J. Phys. Chem. A* **2012**, *116*, 4388−4395.
(18) Raja, I. A.; Gobre, V. V.; Pinjari, R. V.; Gejji, S. P. *J. Mol. Model.* **2014**, *20*, 2138.
(19) Carlqvist, P.; Maseras, F. *Chem. Commun.* **2007**, 748−750.
(20) Xu, L.; Hua, W.; Hua, S.; Li, J.; Li, S. *J. Org. Chem.* **2013**, *78*, 3577−3582.
(21) Balcells, D.; Maseras, F. *New J. Chem.* **2007**, *31*, 333−343.
(22) Norskov, J. K.; Bligaard, T.; Rossmeisl, J.; Christensen, C. H. *Nat. Chem.* **2009**, *1*, 37−46.
(23) Rush, L. E.; Pringle, P. G.; Harvey, J. N. *Angew. Chem., Int. Ed.* **2014**, *53*, 8672−8676.
(24) Mock, W. L.; Irra, T. A.; Wepsiec, J. P.; Adhya, M. *J. Org. Chem.* **1989**, *54*, 5302−5308.
(25) Mock, W. L.; Irra, T. A.; Wepsiec, J. P.; Manimaran, T. L. *J. Org. Chem.* **1983**, *48*, 3619−3620.
(26) Assaf, K. I.; Nau, W. M. *Chem. Soc. Rev.* **2015**, *44*, 394−418.
(27) Freeman, W. A.; Mock, W. L.; Shih, N. Y. *J. Am. Chem. Soc.* **1981**, *103*, 7367−7368.
(28) Lagona, J.; Mukhopadhyay, P.; Chakrabarti, S.; Isaacs, L. *Angew. Chem., Int. Ed.* **2005**, *44*, 4844−4870.
(29) Pichierri, F. *J. Mol. Struct.: THEOCHEM* **2006**, *765*, 151−152.
(30) Huisgen, R. *Angew. Chem., Int. Ed. Engl.* **1963**, *2*, 633−645.
(31) Gothelf, K. V.; Jorgensen, K. A. *Chem. Rev.* **1998**, *98*, 863−909.
(32) Kolb, H. C.; Finn, M. G.; Sharpless, K. B. *Angew. Chem., Int. Ed.* **2001**, *40*, 2004−2021.
(33) El-Sheshtawy, H. S.; Bassil, B. S.; Assaf, K. I.; Kortz, U.; Nau, W. M. *J. Am. Chem. Soc.* **2012**, *134*, 19935−19941.

(34) Moghaddam, S.; Inoue, Y.; Gilson, M. K. *J. Am. Chem. Soc.* **2009**, *131*, 4012−4021.

(35) Moghaddam, S.; Yang, C.; Rekharsky, M.; Ko, Y. H.; Kim, K.; Inoue, Y.; Gilson, M. K. *J. Am. Chem. Soc.* **2011**, *133*, 3570−3581.

(36) Gadde, S.; Batchelor, E. K.; Weiss, J. P.; Ling, Y.; Kaifer, A. E. *J. Am. Chem. Soc.* **2008**, *130*, 17114−17119.

(37) Venkataramanan, N. S.; Ambigapathy, S.; Mizuseki, H.; Kawazoe, Y. *J. Phys. Chem. B* **2012**, *116*, 14029−14039.

(38) Frisch, M. J.; Trucks, G. W.; Schlegel, H. B.; Scuseria, G. E.; Robb, M. A.; Cheeseman, J. R.; Scalmani, G.; Barone, V.; Mennucci, B.; Petersson, G. A.; Nakatsuji, H.; Caricato, M.; Li, X.; Hratchian, H. P.; Izmaylov, A. F.; Bloino, J.; Zheng, G.; Sonnenberg, J. L.; Hada, M.; Ehara, M.; Toyota, K.; Fukuda, R.; Hasegawa, J.; Ishida, M.; Nakajima, T.; Honda, Y.; Kitao, O.; Nakai, H.; Vreven, T.; Montgomery, J. A., Jr.; Peralta, J. E.; Ogliaro, F.; Bearpark, M.; Heyd, J. J.; Brothers, E.; Kudin, K. N.; Staroverov, V. N.; Kobayashi, R.; Normand, J.; Raghavachari, K.; Rendell, A.; Burant, J. C.; Iyengar, S. S.; Tomasi, J.; Cossi, M.; Rega, N.; Millam, J. M.; Klene, M.; Knox, J. E.; Cross, J. B.; Bakken, V.; Adamo, C.; Jaramillo, J.; Gomperts, R.; Stratmann, R. E.; Yazyev, O.; Austin, A. J.; Cammi, R.; Pomelli, C.; Ochterski, J. W.; Martin, R. L.; Morokuma, K.; Zakrzewski, V. G.; Voth, G. A.; Salvador, P.; Dannenberg, J. J., ;Dapprich, S.; Daniels, A. D.; Farkas, A.; Foresman, J. B.; Ortiz, J. V.; Cioslowski, J.; Fox, D. J. *Gaussian 09 Revision D.01*; Gaussian Inc., Wallingford, CT, 2009.

(39) Grimme, S. *J. Comput. Chem.* **2006**, *27*, 1787−1799.

(40) Francl, M. M.; Pietro, W. J.; Hehre, W. J.; Binkley, J. S.; Gordon, M. S.; DeFrees, D. J.; Pople, J. A. *J. Chem. Phys.* **1982**, *77*, 3654−3665.

(41) Grimme, S.; Ehrlich, S.; Goerigk, L. *J. Comput. Chem.* **2011**, *32*, 1456−1465.

(42) Goerigk, L.; Grimme, S. *Phys. Chem. Chem. Phys.* **2011**, *13*, 6670−6688.

(43) Krishnan, R.; Binkley, J. S.; Seeger, R.; Pople, J. A. *J. Chem. Phys.* **1980**, *72*, 650−654.

(44) Marenich, A. V.; Cramer, C. J.; Truhlar, D. G. *J. Phys. Chem. B* **2009**, *113*, 6378−6396.

(45) Biedermann, F.; Nau, W. M.; Schneider, H.-J. *Angew. Chem., Int. Ed.* **2014**, *53*, 11158−11171.

(46) Boys, S. F.; Bernardi, F. *Mol. Phys.* **1970**, *19*, 553−566.

(47) Braun, W.; Herron, J. T.; Kahaner, D. K. *Int. J. Chem. Kinet.* **1988**, *20*, 51−62.

(48) Wachsstock, D. Tenua: The Kinetics Simulator for Java; http://bililite.com/tenua.

(49) Eyring, H. *J. Chem. Phys.* **1935**, *3*, 107−115.

(50) Mock, W. L.; Shih, N. Y. *J. Org. Chem.* **1986**, *51*, 4440−4446.